Probing medium-range structural correlations by fluctuation microscopy

2007 J. Phys.: Condens. Matter 19 455201

(http://iopscience.iop.org/0953-8984/19/45/455201)

IOP PUBLISHING JOURNAL OF PHYSICS: CONDENSED MATTER

J. Phys.: Condens. Matter **19** (2007) 455201 (10pp) doi:10.1088/0953-8984/19/45/455201

Probing medium-range structural correlations by fluctuation microscopy

M M J Treacy[1], D Kumar[1], A Rougée[1,5], G Zhao[2], P R Buseck[2,3], I McNulty[4], L Fan[4,6], C Rau[4,7] and J M Gibson[4]

[1] Department of Physics, Arizona State University, Tempe, AZ 85287, USA
[2] Arizona State University, School of Earth and Space Exploration, Tempe, AZ 85287, USA
[3] Department of Chemistry/Biochemistry, Arizona State University, Tempe, AZ 85287, USA
[4] Argonne National Laboratory, 9700 South Cass Avenue, Argonne, IL 60439, USA

E-mail: treacy@asu.edu

Received 23 July 2007, in final form 24 July 2007
Published 24 October 2007
Online at stacks.iop.org/JPhysCM/19/455201

Abstract

We outline recent advances in the fluctuation microscopy technique for probing medium-range structural correlations in disordered materials. The technique was originally developed for electron microscopy, but has now been extended to optical and x-ray microscopies.

We show that fluctuation microscopy can detect trace quantities of C_{60} in a disordered graphite matrix, even though the diffraction signature from the C_{60} is essentially undetectable. This result indicates that the technique can be used to discern dilute distributions of macromolecules in an otherwise disordered matrix.

We also report preliminary studies of interferometric fluctuation microscopy using cross-correlations in diffraction between coherent double probes. This is a form of holography where the diffraction patterns from two neighboring regions are allowed to overlap and interfere. Young's fringes appear wherever both regions scatter strongly. The cross-correlation can be examined as a function of probe separation to estimate a structure correlation length. This method holds much promise for studying medium-range order, since it isolates the essential four-body terms underpinning the fluctuation microscopy technique.

(Some figures in this article are in colour only in the electronic version)

[5] Present address: 1920 Hunnewell St, Honolulu, HI 96822, USA.
[6] Present address: Northwestern University, 633 Clark Street, Evanston, IL 60208, USA.
[7] Present address: Diamond Light Source Ltd, Didcot, Oxfordshire, OX11 0DE, UK.

0953-8984/07/455201+10$30.00

1. Introduction

Fluctuation microscopy is a spatially resolved scattering technique that is especially sensitive to medium-range structural correlations in disordered materials. The sensitivity is due to the fact that the fluctuation microscopy signal contains information about four-body correlations within the sample [1–3]. Pure diffraction, where the incident plane wave inherently contains no spatial resolution, gives a two-body signal that depends only on correlations between pairs of scatterers [4]. The fluctuation microscopy method can be thought of as containing information about pair–pair correlations, hence its sensitivity to medium-range order [5, 6]. Here, we define the medium-range order at the atomic scale to mean length scales between about 0.5 and 3.0 nm. For nanoscale and macroscale systems, this translates to mean ordering between about three and 20 nearest-neighbor distances.

Fluctuation microscopy, as a technique, is over a decade old now. The method, and some of the early results, have been described in detail in a recent review [3]. Fluctuation microscopy, like most new techniques, is evolving. In this article, we provide a brief review of the technique, and overview some of the recent experiments, insights, and methodologies that have emerged since that earlier review.

2. What is fluctuation microscopy?

The 'fluctuations' in fluctuation microscopy refer to the differences in scattering between neighboring regions of the sample. Fluctuation microscopy is the spatial analogue of correlation spectroscopy. To our knowledge, both time- and spatially resolved experiments have not yet been conducted.

Since fluctuation microscopy relies primarily on diffraction, which is a two-body pair correlated signal [4, 7], its ability to extract four-body pair–pair correlations might seem confusing at first. The higher-order correlations emerge because fluctuation microscopy is a spatially resolved diffraction technique. The incident waves are not pure plane waves, but are converging—that is, focused—onto the sample. The statistics of the scattering between probed volumes give rise to the higher-order correlations. The simplest statistical parameters are the mean and variance of the scattering, although these are by no means the only statistical moments available.

There are two equivalent methods for obtaining fluctuation microscopy data [3]. The first method is to collect dark-field images formed by tilting the illumination (which may be a plane wave) and collecting the scattering into an axial objective aperture. An objective lens forms an image that is essentially a spatial map of the scattering strength into the diffraction vectors subtended by the objective aperture. A series of images $I(\boldsymbol{r}, \boldsymbol{Q}_i)$ can be collected as a function of the scanned illumination tilt vector, $\boldsymbol{Q}_i$. The image, of course, already contains the full set of sample locations, $\boldsymbol{r} \equiv \{\boldsymbol{r}_i\}$. The image resolution, or point spread function, is controlled by the objective aperture width; the narrower the aperture, the wider the point spread function. In the limit of a point aperture that collects a narrow range of diffraction vectors, there is no spatially resolved information and we have essentially a standard Fraunhofer diffraction experiment. Conversely, a wide objective aperture provides a high-resolution image, capable of resolving detail at length scales comparable to, or shorter than, the spacing between scatterers. However, since the aperture collects a wide range of scattering vectors, it resolves poorly the contributions due to particular diffraction vectors. Each image, $I(\boldsymbol{r}, \boldsymbol{Q}_i)$, from a disordered sample tends to be speckled, and it is the statistics of the image speckle as a function of the full set of scattering vectors $\boldsymbol{Q}$ that is examined.

In the second method, a probe is formed on the sample, centered at location $\boldsymbol{r}_i$, and a series of diffraction patterns, $I(\boldsymbol{r}_i, \boldsymbol{Q})$, are collected [8–10]. In this modality, each diffraction pattern

contains the full range of diffraction vectors, $\boldsymbol{Q} \equiv \{\boldsymbol{Q}_i\}$, for each sample location $\boldsymbol{r}_i$. Now it is the diffraction pattern, $I(\boldsymbol{r}_i, \boldsymbol{Q})$, that exhibits speckle.

In principle, the two methods accumulate the same four-dimensional data set, $I(\boldsymbol{r}, \boldsymbol{Q})$—two dimensions each for $\boldsymbol{r}$ and $\boldsymbol{Q}$. However, in practice, the scanned variable tends to be undersampled in order to avoid a glut of data.

A simple measure of the fluctuations in the full data is to compute the variance of the intensity with respect to the spatial coordinate $\boldsymbol{r}$, and to inspect its dependence on diffraction vector $\boldsymbol{Q}$. Since most independent scatterers exhibit a form factor that tends to fall off with increasing Q, it is helpful to normalize the variance by dividing by the square of the mean intensity:

$$V_{\mathrm{N}}(\boldsymbol{Q}) = \frac{\langle I^2(\boldsymbol{r}, \boldsymbol{Q})\rangle_{\mathrm{r}}}{\langle I(\boldsymbol{r}, \boldsymbol{Q})\rangle_{\mathrm{r}}^2} - 1. \tag{1}$$

The subscript r indicates that the average is over the spatial coordinate.

The key point here is that a random distribution of point scatterers will produce plots $V_{\mathrm{N}}(\boldsymbol{Q})$ that contain no special peaks in $\boldsymbol{Q}$-space. It turns out that, even for randomly close-packed spheres and continuous random networks, there are no pronounced features in the $V_{\mathrm{N}}(\boldsymbol{Q})$ plots. If local ordering is present, such as small regions of cubic close packing, peaks appear at those $\boldsymbol{Q}$ vectors where non-random coherent scattering occurs. The peaks are broadened in part because the scattering region is small, and because of the angular width of the objective aperture.

Optimally, the resolution (i.e. the image point spread function) should be comparable to the characteristic width of the structural correlations in the sample. If the resolution is too high (smaller than the typical separation between scatterers), then lateral coherent scattering is suppressed. Only the coherent scattering between objects aligned along columns parallel to the probe remains. Conversely, if the point spread function is much wider than the typical structural correlation width, then the scattering is being averaged over many domains and the scattering variations across the probe average out. However, when the resolution is comparable to the correlation width, then the variability in scattering between pixels is close to maximum. This 'Goldilocks' effect, where the variance is maximal when the resolution is 'just right', offers a simple method for estimating the structural correlation length scale, by varying the resolution in order to seek the maximal variability. In the TEM, it is difficult to vary the resolution continuously, although in principle a suite of discrete objective apertures could be employed. The flexibility of the probe-forming electron optics in the scanning transmission electron microscope (TEM) allows the coherent probe width to be varied over a limited range without the need to change apertures.

In the TEM, fluctuation electron microscopy has been found to be useful for studying medium-range order in amorphous semiconductors [5, 6, 11–13], carbons [14–16] and intermetallic glasses [17–20]. Here, we outline some recent advances made in the fluctuation microscopy technique using electrons, x-rays and visible light to study structural correlations at a wide range of length scales.

3. Fluctuation electron microscopy as a tool for detecting dilute distributions of macromolecules

Medium-range order can be manifested in many ways. For example, paracrystallinity has been observed in amorphous tetrahedral semiconductors. This particular form of paracrystallinity resembles a compact of nanocrystalline grains with the diamond structure (and possibly also the hexagonal lonsdaleite topology) embedded within a continuous random network. The nanocrystalline grains are under stress and are deformed from the ideal lattice positions.

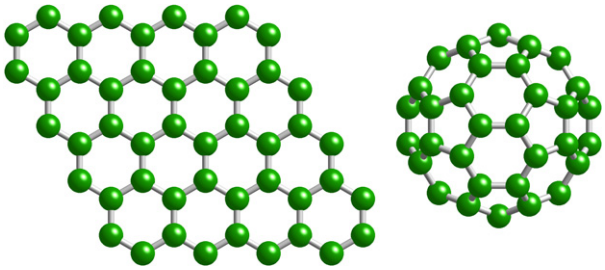

Figure 1. Comparison of the structures of a 45-atom graphite fragment (left) and a C_{60} molecule (right). The graphite sheet is viewed parallel to the 6 mm point symmetry axis, and the C_{60} is viewed parallel to a 2 mm axis.

In a recent study we have found that fluctuation microscopy is remarkably sensitive to the trace presence of C_{60} molecules within an otherwise highly disordered partially graphitized matrix [16].

It had been shown earlier that crystalline C_{60} can occur in a natural carbonaceous rock, shungite [21]. Shungite is almost 100% pure carbon. It was clear from diffraction and high-resolution bright-field imaging studies that shungite contains a highly defective form of graphite, with many bent and interrupted graphite planes [22]. One remarkable bright-field image showed an extended crystal of C_{60} [21]. Although sightings of C_{60} crystals are rare in shungite, time-of-flight mass spectroscopy confirmed that trace quantities of C_{60} and C_{72} occur in some samples [21].

A fullerene molecule within an otherwise disordered carbon matrix is a locally ordered region of carbon. Thus, a dilute dispersion of C_{60} in a defective graphitic matrix is equivalent to local medium-range order on the length scale of about 0.8 nm, which is the diameter of the C_{60} molecule measured from carbon center to carbon center. Figure 1 compares a 45-atom fragment of graphite with a C_{60} molecule. Although both are three-coordinated carbon networks with similar C–C bond distances, the diffraction patterns from each are quite distinct. Figure 2(a) shows line traces through the calculated mean diffraction patterns for graphite and C_{60}. The calculations assume a Gaussian point spread function equivalent to a resolution of 1.5 nm, which is the principle contribution to the peak broadening. The patterns represent a radial line trace of the powder pattern created by incoherently adding the diffracted intensities from a large ensemble of randomly oriented fragments, such as those shown in figure 1. Figure 2(b) shows the normalized variance of the ensemble of diffraction patterns.

A striking feature of the normalized variance is that C_{60} exhibits a pronounced peak near 7.1 nm^{-1}, which does not appear in the normalized variance for graphite. Intriguingly, there is no corresponding peak in the mean diffraction pattern from C_{60} at this location. In fact, there is a pronounced dip in this region for both C_{60} and graphite. The location of this variance peak corresponds to a spacing of $\sim$0.14 nm, which is close to the C–C bond distance in graphite and C_{60}. In graphite, reflections from this spacing (equivalent to $\{3/2\ 0\ 0\}$ planes) are forbidden because adjacent C–C pairs are staggered by half a C–C bond distance, ensuring destructive interference. However, in C_{60}, there are special orientations, such as is shown in figure 1, where significant intensity at this location can appear. In a statistical ensemble of randomly oriented C_{60}, some molecules will be oriented correctly for strong scattering into this reflection, enhancing speckle near $Q \approx 7.1\ nm^{-1}$.

Experimental fluctuation electron microscopy (FEM) data (see figure 3) confirm that samples of pure C_{60} and shungite both exhibit pronounced peaks at the special $Q \approx 7.1\ nm^{-1}$

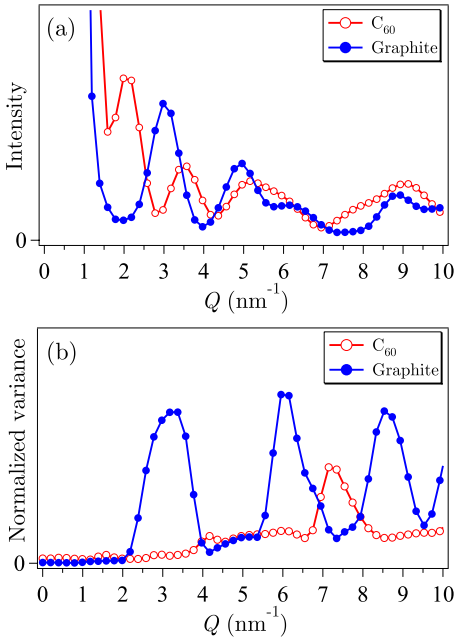

Figure 2. (a) Mean diffraction profile for randomly oriented ensembles of graphite (filled circles) and C_{60} (open circles). The calculations assume a 1.5 nm wide Gaussian point spread function. (b) Normalized variance of diffracted intensity for randomly oriented ensembles of graphite (filled circles) and C_{60} (open circles).

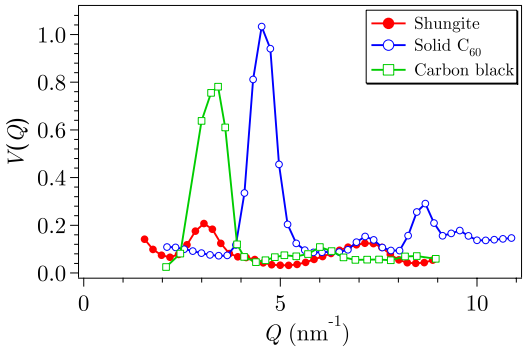

Figure 3. Experimental normalized variance plots for a pure sample of C_{60} (open circles), a shungite sample (filled circles) and a sample of carbon black (open squares). Both the shungite and C_{60} samples exhibit the same strong peak near $Q \approx 7.1$ nm^{-1}. The carbon black sample, which is a form of disordered graphite, shows only graphite peaks and no peak at $Q \approx 7.1$ nm^{-1}.

diffraction vector, whereas textured graphite (not shown) and graphitic carbon black (shown) do not.

It is clear from extensive studies of high-resolution bright-field images that shungite does indeed contain occasional isolated fullerenes with diameters less than 1 nm. Although those sightings are rare, they affirm the claims based on FEM data. The conclusion from this study is that fluctuation microscopy can be remarkably sensitive to the presence of trace quantities of C_{60}. Our studies show that the distribution of C_{60} is heterogeneous. The concentration of C_{60} can vary significantly over distances as short as 1 μm. At present we do not yet know how to

quantify the concentration of C_{60} based on the FEM data alone, because we still lack a model that allows us to invert the variance data. Our simulations suggest that the $Q \approx 7.1$ nm^{-1} peak is unique to C_{60}. For larger fullerenes, such as C_{70} and C_{72} etc, the peak moves significantly to higher Q, and then vanishes. These simulations suggest that our experimental results are specific to the curvature associated with C_{60}, and are not a general indicator of fullerenes.

4. Interferometric fluctuation microscopy

The sensitivity of fluctuation microscopy to medium-range order arises because the variance signal probes higher-order correlations, such as atom pair–pair correlations. In its original form, fluctuation microscopy uses a spatially coherent broadened probe, or point spread function, to examine many sample volumes. This is not the only method available for probing higher-order correlations. An alternative, but slightly more experimentally challenging, approach is to illuminate the sample with a pair of smaller mutually coherent probes. Each probe generates a micro-diffraction pattern from the illuminated region. The two diffraction patterns then interfere to produce a Young's fringe intensity modulation wherever both patterns have significant scattering amplitude at the same scattering vector. If the first probe produces a diffracted wavefunction $\psi_A(\boldsymbol{Q})$, and the second probe produces a diffracted wavefunction $\psi_B(\boldsymbol{Q})$, then, for a probe separation $\boldsymbol{R}$, the resultant diffraction intensity is

$$I = |\psi_A|^2 + |\psi_B|^2 + \psi_A^* \psi_B \exp(-2\pi \mathrm{i} \boldsymbol{Q} \cdot \boldsymbol{R}) + \psi_A \psi_B^* \exp(2\pi \mathrm{i} \boldsymbol{Q} \cdot \boldsymbol{R}). \quad (2)$$

The first two terms are the incoherent sum of the separate diffraction patterns from each probe. The second two terms are the interference terms due to the mutual coherence of the displaced probes.

Figure 4(a) illustrates coherent double probes on a thin amorphous sample, and figure 4(b) presents a simulation of the mean kinematical diffraction pattern obtained when such a probe pair is scanned across a model containing medium-range order. In the simulation, the probe widths are 0.5 nm and are separated by $R = 1.0$ nm. The model is for amorphous silicon containing ∼1.5 nm wide paracrystallites. The central diffraction disk shows strong interference fringes because both probes have strong zero-order beams. Interference fringes persist in the diffraction rings because there is significant structural correlation between the material under each probe. As the probe separation increases, the fringe spacing decreases, and the fringe modulation in the diffraction rings diminishes due to the fact that the two probes tend to be exploring inherently different structures more often.

We have conducted trial experiments with double probes using both x-rays and laser light. Figure 5(a) shows the mean diffraction pattern obtained with He–Ne laser light at 632.8 nm from a test sample comprising a monolayer of 20 μm diameter latex spheres on a glass slide. The sample was scanned across a coherently illuminated vertically separated double pinhole, where each pinhole had a diameter of 100 μm and they were separated by 400 μm. The sample was about 200 μm from the pinholes, so propagation broadening effects are small. Optical microscopy shows that the typical ordered region in the sample was about 500 μm across. About 1600 diffraction patterns were obtained using step sizes of 50 μm along perpendicular x and y directions—this being the nominal Nyquist sampling rate for a single 100 μm pinhole. The mean pattern shows finely spaced horizontal interference fringes due to the approximately vertical separation of the two pinholes. Figure 5(b) shows the Fourier transform of this diffraction pattern. As expected, satellite patterns corresponding to the Fourier transforms of the cross-terms $\psi_A^* \psi_B$ and $\psi_A \psi_B^*$ are centered at the $\pm\boldsymbol{R}$ positions. In addition, satellite spots appear at the $\pm 2\boldsymbol{R}$ harmonics. These are due primarily to nonlinearity in the signal detection such as pixel saturation in the CCD camera, particularly in the central beam, and shot noise, which has a nonlinear dependence on intensity.

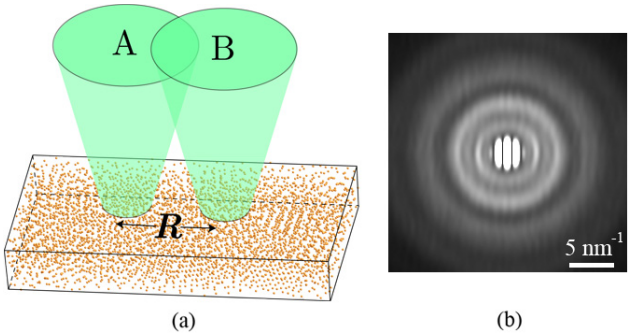

Figure 4. (a) Illustration of a thin disordered sample being scanned by a coherent double probe. (b) Calculation of the mean diffraction pattern obtained when a coherent double probe is scanned across a model of paracrystalline silicon. Young's interference fringes appear wherever there is significant overlap in diffraction amplitude from both probes.

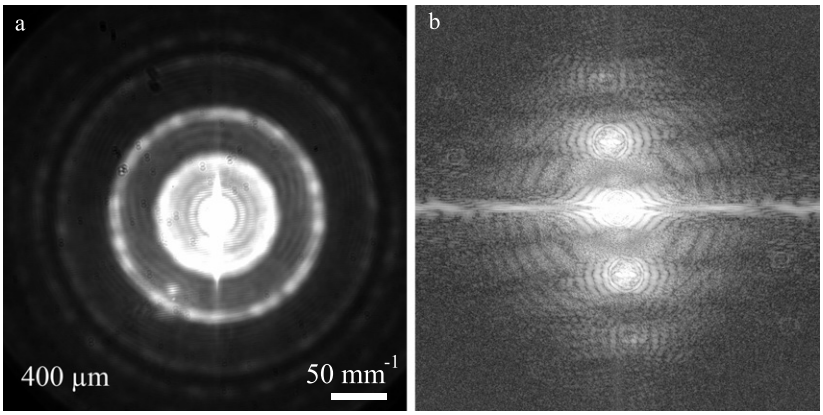

Figure 5. Optical data from a sample comprising a disordered (polycrystalline) monolayer of 20 μm diameter latex beads on glass. He–Ne laser light of wavelength 632.8 nm was used. Here, two pinholes of diameter 100 μm and vertical separation of 400 μm were scanned across the sample to collect 1600 diffraction patterns. (a) The mean diffraction pattern, which has finely spaced horizontal Young's fringes. (b) The Fourier transform of the mean diffraction pattern showing the $\pm\boldsymbol{R}$ satellite spots corresponding to the interference fringes. In addition, there are faint satellite spots at $\pm 2\boldsymbol{R}$, which are due to nonlinearity in the detected signal.

If one of the first-order satellite spots in the Fourier transform is masked by a circular aperture of radius less than R, and then back-transformed into Q-space, we obtain a filtered version of the diffraction cross-terms $\mathrm{Re}\{\psi_{\mathrm{A}}^{*}\psi_{\mathrm{B}}\}$. The resultant interference patterns represent the cross-correlation of the diffraction patterns under the two spatially separated probes. If the two diffracted signals have no features in common, then there is only a central spot. If the two patterns have scattering features in common, then those features will persist in the interference pattern. For example, a perfectly ordered crystal will produce similar diffraction amplitudes under the two probes at all separations, provided that the two probes are mutually coherent. The interference patterns will resemble the diffraction pattern from a single probe.

Figure 6 shows optical interference patterns for He–Ne laser light ($\lambda = 632.8$ nm) for two test samples comprising monolayers of 20 μm latex spheres on a glass slide, similar to that used in figure 5. The double pinholes used were 100 μm in diameter and were separated

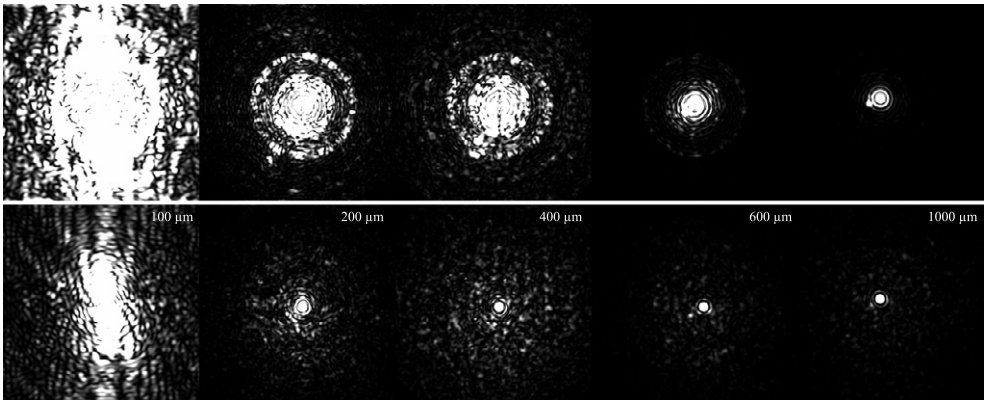

Figure 6. Optical cross-correlation patterns $\mathrm{Re}\{\psi_A^*\psi_B\}$ for two samples comprising monolayers of disordered 20 μm spheres. The top row is for a sample with a characteristic polycrystallite width of ~500 μm. The bottom row is for a sample with a characteristic polycrystallite width of ~300 μm. The five columns correspond to different spacings, R, between two 100 μm diameter pinholes. From left to right, the spacings are $R = 100$ μm, 200 μm, 400 μm, 600 μm and 1000 μm, respectively.

by $R = 100$, 200, 400, 600 and 1000 μm. The pinholes were ~200 μm from the sample to minimize the beam dispersion at the sample due to pinhole diffraction. The top row is for a sample that, from optical microscopy measurements, is polycrystalline with a characteristic domain size of about 500 μm. The bottom row is for a similar sample that had a characteristic domain size of about 300 μm. The five columns correspond to the five probe separations, increasing in R from left to right. The patterns at $R = 100$ μm (left) lack circular symmetry because the probes are close and the masking aperture does not fully isolate the contributions from the cross-terms and the $|\psi_A|^2 + |\psi_B|^2$ terms.

As expected, the interference patterns for the more disordered sample (lower row) decay faster with probe separation than do the patterns for the more ordered sample (top row). The decay rate appears to be faster at the higher Q values. The zero-order intensity remains approximately constant, indicating that the two probes remain mutually coherent.

The optical experiments were conducted as proof-of-principle experiments for synchrotron x-ray experiments. In addition, we have conducted simulations using models of disorder, such as that shown in figure 4. Both the optical experiments and the modeling indicate that this interferometric fluctuation microscopy method holds much promise for obtaining quantitative details about the order length scales in a sample.

For optical and electron experiments, focused double probes can be formed using optical devices such as Fresnel biprisms. Biprism wires are already used for electron holography experiments [23]. In fact, the interference patterns are a form of holography. However, unlike normal holography, the reference beam is not an unscattered beam, but a reference *scattered* beam from another area of the sample.

For x-ray experiments, double pinholes have been constructed with diameters as small as 0.1 μm. Alternatively, two zone plates can be placed in close proximity and the lateral separation can be varied continuously. X-ray zone plates tend to be transparent, and thus they both can produce well-focused beams at the sample. The zone plates can be slid over one another, making them almost coplanar. Their separation can easily lie well within the depth of focus of each zone plate, so both probes can be considered to be sufficiently well focused on the sample.

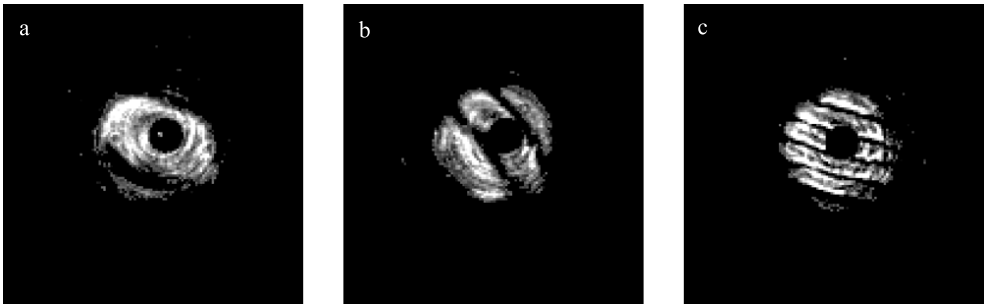

Figure 7. Interference patterns in the central diffraction spot produced by two overlapping zone plates with different transverse separations: (a) single fringe in center of the pattern, corresponding to $R \approx 160$ nm separation between probes; (b) three fringes at $R \approx 390$ nm probe separation; (c) five fringes at $R \approx 650$ nm probe separation.

Figure 7 shows three x-ray diffraction patterns obtained with double zone plates that were separated by 160 nm, 390 nm and 650 nm, respectively. Strong Young's interference fringes appear across the zero-order disk. The zone plates are mostly transparent to x-rays, and consequently both retain their ability to focus x-rays that are incident across their full diameter. There are still important details to be worked out in these experiments. For example, poor signal-to-noise in the scattering generates higher-order harmonics in the Fourier transform that will complicate the analysis. However, it is clear that this interferometric approach can provide important additional information about pair–pair structural correlations.

The method that we describe is similar to the differential interference contrast x-ray microscopy technique of Kaulich *et al* [24], who use it to enhance image contrast in the scanning transmission x-ray microscope. In that mode, a configured CCD detector is also needed, which is not the case in our experiments.

5. Conclusions

Fluctuation microscopy is an evolving technique. As we show here, in some instances it can be a sensitive method for detecting and identifying dilute distributions of macromolecules within a matrix. In principle, that matrix does not need to be disordered. In the case of the shungite example that we show here, trace amounts of C_{60} could be detected in a disordered graphitic carbon matrix. Modeling shows that, for maximum sensitivity, the macromolecule should be capable of scattering strongly into scattering vectors that have weak intensity from the matrix.

The sensitivity to medium-range order arises from the fact that the normalized variance depends on higher-order correlations, up to four-body terms. Theory shows that the four-body terms appear as pair–pair correlations. Here we show that the use of coherent double probes in interferometric fluctuation microscopy may allow us to explore the pair–pair correlations more systematically.

These improvements in experimental methods offer the possibility of increasing the information obtained from disordered samples, and may help to make the technique more accessible to theoretical modeling.

Acknowledgments

The authors wish to thank D J Paterson and M D de Jonge for useful discussions.

References

[1] Treacy M M J and Gibson J M 1996 Variable coherence microscopy: a rich source of structural information from disordered materials *Acta Crystallogr.* A **52** 212

[2] Voyles P M and Abelson J R 2003 Medium-range order in amorphous silicon measured by fluctuation electron microscopy *Sol. Energy Mater. Sol. Cells* **78** 85–113

[3] Treacy M M J, Gibson J M, Fan L, Paterson D J and McNulty I 2005 Fluctuation microscopy: a probe of medium range order *Rep. Prog. Phys.* **68** 2899–944

[4] Warren B E 1959 *X-ray Diffraction* (Reading, MA: Addison-Wesley)

[5] Gibson J M and Treacy M M J 1997 Diminished medium-range order observed in annealed amorphous germanium *Phys. Rev. Lett.* **78** 1074

[6] Gibson J M and Treacy M M J 1998 Paracystallites found in evaporated amorphous tetrahedral semiconductors *J. Non-Cryst. Solids* **231** 99–110

[7] Billinge S J L 1998 Real-space rietveld: full profile structural refinement of the atomic pair distribution function *Local Structure from Diffraction* ed S J L Billinge and M F Thorpe (New York: Plenum) pp 137–56

[8] Voyles P M and Muller D M 2002 Fluctuation microscopy in the STEM *Ultramicroscopy* **93** 147–59

[9] Fan L, McNulty I, Paterson D, Treacy M M J and Gibson J M 2005 Fluctuation microscopy—a tool for examining medium-range order in noncrystalline systems *Nucl. Instrum. Methods Phys. Res.* B **238** 196–9

[10] Fan L, Paterson D, McNulty I, Treacy M M J and Gibson J M 2007 Fluctuation x-ray microscopy: a novel approach for the structural study of disordered materials *J. Microsc.* **225** 41–8

[11] Gibson J M, Treacy M M J, Voyles P M, Jin H-C and Abelson J R 1998 Structural disorder induced in hydrogenated amorphous silicon by light soaking *Appl. Phys. Lett.* **73** 3093–6

[12] Gerbi J E, Voyles P M, Treacy M M J, Gibson J M, Chen W C, Hauser B J and Abelson J R 2001 Control of medium range order in amorphous silicon via ion and neutral bombardment *Amorphous and Heterogeneous Silicon-Based Thin Films-2001* vol 664, ed M Stutzmann, J B Boyce, J D Cohen, R W Collins and J Hanna (Warrendale, PA: Materials Research Society) p A27.3.1–6

[13] Voyles P M, Gerbi J E, Treacy M M J, Gibson J M and Abelson J R 2001 Increased medium-range order in amorphous silicon with increased substrate temperature *Phys. Rev. Lett.* **86** 5514–8

[14] Johnson J A, Woodford J B, Chen X, Anderson J, Erdemir A and Fenske G F 2004 Insights into 'near-frictionless carbon films' *J. Appl. Phys.* **95** 7765–71

[15] Chen X, Sullivan J P, Friedmann T A and Gibson J M 2004 Fluctuation microscopy studies of medium-range ordering in amorphous diamond-like carbon films *Appl. Phys. Lett.* **84** 2823–5

[16] Zhao G, Rougée A, Buseck P R and Treacy M M J 2007 Fluctuation electron microscopy evidence for a dilute disordered distribution of C_{60} and other fullerene macromolecules in a natural carbonaceous rock, in preparation

[17] Li J, Gu X and Hufnagel T C 2001 Medium-range order in metallic glasses studied by fluctuation microscopy *Microsc. Microanal.* **7** (Suppl. 2: Proceedings) 1260–1

[18] Hufnagel T C, Fan C, Ott R T, Li J and Brennan S 2002 Controlling shear band behavior in metallic glass through microstructural design *Intermetallics* **10** 1163–6

[19] Li J, Gu X and Hufnagel T C 2003 Using fluctuation microscopy to characterize structural order in metallic glass *Microsc. Microanal.* **9** 509–15

[20] Stratton W G, Hamann J, Perepezko J H, Voyles P M, Khare S V and Mao X 2005 Aluminum nanoscale order in amorphous $Al_{92}Sm_8$ measured by fluctuation electron microscopy *Appl. Phys. Lett.* **86** 141910

[21] Buseck P R, Tsipursky S J and Hettich R 1992 Fullerenes from the geological environment *Science* **257** 215–7

[22] Kovalevski V V, Buseck P R and Cowley J M 2001 Comparison of carbon in shungite rocks to other natural carbons: an x-ray and tem study *Carbon* **39** 243–56

[23] Tonomura A 1999 *Electron Holography* (Berlin: Springer)

[24] Kaulich B, Wilhein T, Di Fabrizio E, Romanato F, Altissimo M, Cabrini S, Fayard B and Susini J 2002 Differential interference contrast x-ray microscopy with twin zone plates *J. Opt. Soc. Am.* A **19** 797–806